Two-pump four-wave mixing in silicon waveguides for broadband wavelength conversion

Shiming Gao [*a,b], Lizhong Cao[a], En-Kuang Tien[b], Yuewang Huang[b], Qiang Liu[a], Qi Song[b], Salih K. Kalyoncu[b], Sailing He[a], Ozdal Boyraz[b]
[a]Centre for Optical and Electromagnetic Research, State Key Laboratory of Modern Optical Instrumentation, Zhejiang University, Hangzhou 310058, China
[b]Advanced Photonics Device and System Laboratory, Department of Electrical Engineering and Computer Science, University of California, Irvine, California 92697, USA

ABSTRACT

Four-wave mixing (FWM) in silicon waveguides is considered to be a promising effect to realize the wavelength conversion function for wavelength-division-multiplexing optical communication systems. Compared to the degenerate FWM with a single pump, the nondegenerate FWM with two pumps shows more flexibility in phase-matching condition and has more opportunities to acquire broader conversion bandwidth. The bandwidth enhancement is theoretically analyzed for the two-pump FWM and an enhancement of 25% is experimentally demonstrated. Also, an ultra-broadband wavelength conversion is presented based on two-pump FWM by fixing one pump near the signal and scanning the other pumps.

Keywords: Four-wave mixing, wavelength conversion, silicon waveguide, two pumps

1. INTRODUCTION

All-optical signal processing based on nonlinear effects in all kinds of nonlinear media is considered to be essential in next generation optical communication systems. In particular, four-wave mixing (FWM) is the promising solution for all-optical wavelength conversion due to its high speed and strict transparency [1]. The wavelength conversion operation has been well investigated based on FWM in highly nonlinear fibers [2] and semiconductor optical amplifiers [3]. Recently, the observation of FWM in silicon waveguides opened the door to realize high-density integrated wavelength converters due to the strong light confinement and the high nonlinear Kerr coefficient of silicon [4].

To achieve a viable solution for real-life applications, broad conversion bandwidth is a critical parameter. Many efforts have been made to improve the conversion bandwidth such as optimizing the waveguide geometries [5] or designing special waveguide structures [6]. FWM can be divided into degenerate or nondegenerate FWM according to one or two pumps are used. Most of previous investigations were based on the single-pump FWM. The two-pump FWM were also used to generate multiple idlers around the signal by using a multi-longitudinal-mode pump [7] or multiple mixing sidebands by injecting two pumps and a signal into the silicon waveguide [8]. In principle, the use of single pump in silicon waveguides comes with rigid phase matching since the dominated factors, both the pump wave number and the pump power, are hard to be tuned due to the inherent principle of single-pump FWM and the nonlinear losses. However, the two-pump FWM shows more flexibility to achieve the phase matching since it can be easily tuned by changing the setting of the pump wavelengths [9]. As a result, the conversion bandwidth has the possibility to enhance in the two-pump regime. In this paper, we will analyze and demonstrate the broadband performance of the two-pump FWM by comparing it with the single-pump FWM. In addition, the schemes of pump setting for broadband wavelength conversion will also be theoretically presented and experimentally demonstrated.

* gaosm@zju.edu.cn; Phone 86 571 8820 6524; Fax 86 571 8820 6513.

Photonic Fiber and Crystal Devices: Advances in Materials and Innovations in Device Applications V, edited by Shizhuo Yin, Ruyan Guo, Proc. of SPIE Vol. 8120, 81200O · © 2011 SPIE · CCC code: 0277-786X/11/$18 · doi: 10.1117/12.892882

Downloaded From: http://spiedigitallibrary.org/ on 11/15/2012 Terms of Use: http://spiedl.org/terms

2. THEORETUCAL MODEL

As shown in Fig. 1, when two pumps λ_{p1} and λ_{p2} are injected into the silicon waveguide together with the signal λ_s, nondegenerate FWM will occur and a converted wave λ_c is generated at $1/\lambda_c = 1/\lambda_{p1} + 1/\lambda_{p2} - 1/\lambda_s$. By taking into account the linear propagation loss, two-photon absorption (TPA), and TPA-induced free-carrier absorption (FCA), the coupled equations for the FWM process under the continuous wave or quasi-continuous wave assumption can be expressed as [9]

$$\frac{dA_{p1}}{dz} = -\frac{1}{2}\left(\alpha_{p1} + \alpha_{TPAp1} + \alpha_{FCAp1}\right)A_{p1} + j\gamma_{p1}\left[\left|A_{p1}\right|^2 + 2\left|A_{p2}\right|^2 + 2\left|A_s\right|^2 + 2\left|A_c\right|^2\right]A_{p1} + 2j\gamma_{p1}A_{p2}^* A_s A_c \exp(j\Delta\beta z) \tag{1}$$

$$\frac{dA_{p2}}{dz} = -\frac{1}{2}\left(\alpha_{p2} + \alpha_{TPAp2} + \alpha_{FCAp2}\right)A_{p2} + j\gamma_{p2}\left[2\left|A_{p1}\right|^2 + \left|A_{p2}\right|^2 + 2\left|A_s\right|^2 + 2\left|A_c\right|^2\right]A_{p2} + 2j\gamma_{p2}A_{p1}^* A_s A_c \exp(j\Delta\beta z) \tag{2}$$

$$\frac{dA_s}{dz} = -\frac{1}{2}\left(\alpha_s + \alpha_{TPAs} + \alpha_{FCAs}\right)A_s + j\gamma_s\left[2\left|A_{p1}\right|^2 + 2\left|A_{p2}\right|^2 + \left|A_s\right|^2 + 2\left|A_c\right|^2\right]A_s + 2j\gamma_s A_c^* A_{p1} A_{p2} \exp(-j\Delta\beta z) \tag{3}$$

$$\frac{dA_c}{dz} = -\frac{1}{2}\left(\alpha_c + \alpha_{TPAc} + \alpha_{FCAc}\right)A_c + j\gamma_c\left[2\left|A_{p1}\right|^2 + 2\left|A_{p2}\right|^2 + 2\left|A_s\right|^2 + \left|A_c\right|^2\right]A_c + 2j\gamma_c A_s^* A_{p1} A_{p2} \exp(-j\Delta\beta z) \tag{4}$$

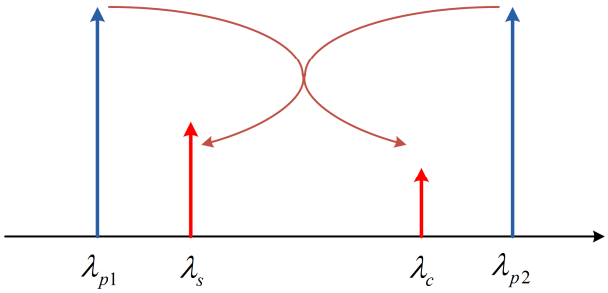

Figure 1. Schematic description of the two-pump FWM process in a silicon waveguide.

In Eqs. (1)-(4), $A_{p1,p2,s,c}(z)$ are the amplitudes of the pumps, the signal, and the converted waves, $\gamma_{p1,p2,s,c}$ are the nonlinear coefficients, $\Delta\beta$ is the linear phase mismatch, $\alpha_{p1,p2,s,c}$ are the linear-loss coefficients, $\alpha_{TPAp1,p2,s,c}$ and $\alpha_{FCAp1,p2,s,c}$ are the nonlinear-loss coefficients caused by the TPA and FCA effects. Mathematically the loss coefficients induced by TPA and FCA can be expressed as

$$\alpha_{TPAi} = \frac{\beta_{TPA}}{A_{eff}}\left(\left|A_i\right|^2 + 2\sum_{m\neq i}\left|A_m\right|^2\right), (i,m = p1,p2,s,c) \tag{5}$$

$$\alpha_{FCAi} = \frac{\sigma_i \beta_{TPA}\tau}{2hcA_{eff}^2}\left(\sum_m \lambda_m \left|A_m\right|^4 + 4\sum_{m\neq n}\frac{\lambda_m\lambda_n\left|A_m\right|^2\left|A_n\right|^2}{\lambda_m + \lambda_n}\right), (i,m = p1,p2,s,c) \tag{6}$$

where $\sigma_{p1,p2,s,c}$ are the FCA cross sections.

Denoting the nonlinear index coefficient of silicon as n_2, the nonlinear coefficients for the involved waves can be calculated as

$$\gamma_i = 2\pi n_2 / \lambda_i A_{eff}\ , (i = p1,p2,s,c) \tag{7}$$

Since all the involved waves are in the same wavelength region, it is reasonable to consider $\alpha_{p1,p2,s,c} = \alpha$, $\sigma_{p1,p2,s,c} = \sigma$, and $\gamma_{p1,p2,s,c} = \gamma$. Supposing $P_{p1,p2,s,c} = |A_{p1,p2,s,c}|^2$, the phase mismatch can be reduced to a simple expression:

Downloaded From: http://spiedigitallibrary.org/ on 11/15/2012 Terms of Use: http://spiedl.org/terms

$$\kappa = \Delta\beta + \gamma\left(P_{p1} + P_{p2}\right) = \beta_s + \beta_c - \beta_{p1} - \beta_{p2} + \gamma\left(P_{p1} + P_{p2}\right) \tag{8}$$

where $\beta_{p1,p2,s,c}$ are the wave numbers of the interacting waves.

Under lossy cases and saturation regimes only numerical solutions are available for Eqs. (1)-(4). In particular the solution to Eq. (4) leads to the definition of the conversion efficiency and the conversion bandwidth. The conversion efficiency, which is defined as

$$\eta(dB) = 10\log_{10}\left[P_c(z)/P_s(0)\right] \tag{9}$$

can be used to determine the conversion bandwidth after solving the coupled equations numerically.

3. BANDWIFTH ENHANCEMENT USING TWO-PUMP FWM

According to Eq. (8), the phase-matching condition of FWM can be freely controlled by the pump spacing when two-pump regime is used and the bandwidth has the chance to be enhanced by setting the pumps. Preliminary calculations are performed in a 1.5-cm-long 300 nm × 650 nm silicon waveguide that corresponds to 0.12158 μm^2 effective mode area. The zero-dispersion wavelength is at 1456 nm. Since the pump power attenuates along the propagation length, the phase mismatch will vary with respect to the distance even though the signal wavelength is fixed. For the single-pump FWM-based wavelength conversion, Fig. 2(a) and 2(b) simulate the phase mismatches for the pump powers of 100 mW and 1000 mW in the above waveguide and the pump wave is assumed at 1550 nm. In our calculation, the linear propagation loss coefficient is assumed to be α = 2.5 dB/cm, the TPA coefficient is β_{TPA} = 0.8 cm/GW for both degenerate and nondegenerate absorptions, the FCA cross section is σ = 1.45 × 10^{-17} cm^2, the effective free-carrier lifetime of carriers is τ = 2 ns, and the nonlinear index coefficient is n_2 = 9 × 10^{-18} m^2/W. One can see that the exact phase-matching curves in Figs. 2(a) and 2(b) are quite similar particularly after propagating 0.5 cm in the silicon waveguide, although the incident pump powers are dramatically different. This effect results in the nonlinear loss due to TPA and FCA, especially where FCA is quadratically proportional to the pump powers. A high incident power will be attenuated rapidly to a relatively low level. As a result, the phase mismatch is slightly changed by the pump power. Figure 2(c) shows the conversion responses for the two cases corresponding to Figs. 2(a) and 2(b) with a signal power of 1 mW. The 3-dB conversion bandwidths are 71.5 and 77.2 nm when 100-mW and 1000-mW pumps are adopted. The bandwidth enhancement is very limited by changing the pump power.

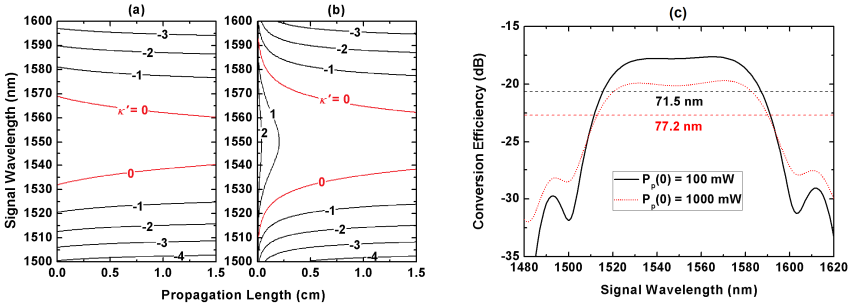

Figure 2. Phase mismatch (in the units of cm^{-1}) of the single-pump FWM as a function of the signal wavelength and the propagation length with the pump power of (a) 100 mW or (b) 1000 mW. (c) Single-pump conversion efficiency as the signal wavelength for the pump power of 100 mW or 1000 mW.

In contrast, the phase mismatch can be greatly changed by setting the two pump wavelengths in the two-pump FWM scheme. When the mean pump wavelength is fixed at 1550 nm, the phase mismatch is calculated by using Eq. (8) with pump spacing of 0 and 61.56 nm, as shown in Figs. 3(a) and 3(b), in which the pump powers are fixed at 100 mW. The linear phase mismatch $\Delta\beta$ is directly determined by the pump wave numbers, that is, the pump wavelengths. One can find that the total phase mismatch is sensitive to the pump wavelength spacing and the perfect phase-matching curves (κ = 0) separate from each other in the contour map with the pump spacing increasing, which means the enhancement of bandwidth. The simulation results of the conversion responses are shown in Fig. 3(c). The 3-dB bandwidth is 70.4 nm when the two pumps are very close, which is quite similar to the single-pump FWM. When the two pumps go away from

Downloaded From: http://spiedigitallibrary.org/ on 11/15/2012 Terms of Use: http://spiedl.org/terms

each other, the bandwidth is enhanced gradually. For the pump wavelength spacing of 61.56 nm, the bandwidth reaches 93.3 nm, which is enhanced by 22.9 nm (33%) compared with the case the two pumps are put closely.

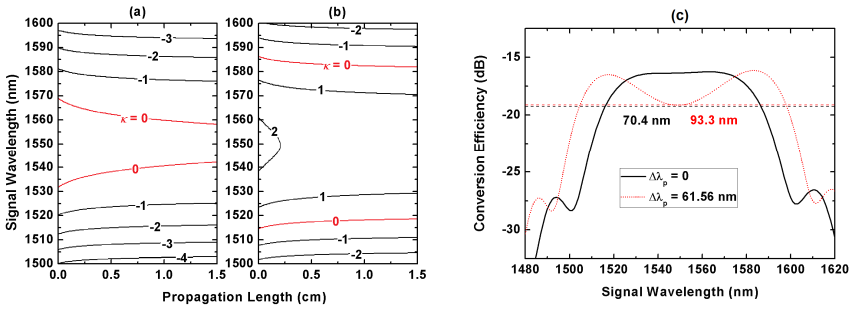

Figure 3. Phase mismatch (in the units of cm^{-1}) of the two-pump FWM as a function of the signal wavelength and the propagation length when the wavelength spacing between the two pumps is (a) 0 and (b) 61.56 nm. (c) Two-pump conversion efficiency as the signal wavelength varies for the pump wavelength spacing of 0 or 61.56 nm.

The nonuniformity of the conversion response is also concomitantly enhanced with the pump spacing of the two-pump FWM increasing since the central signals suffer from larger phase mismatch, which means lower conversion efficiency. For convenience, we define the efficiency difference between the maximum efficiency and the central minimum efficiency as the response nonuniformity. With both pump powers of 100 mW, the conversion bandwidth and the corresponding response nonuniformity are quantitatively simulated versus the pump wavelength spacing, as shown in Fig. 4. One can see that the response nonuniformity is also enhanced together with the conversion bandwidth by separating the two pumps. The response nonuniformity reaches 3 dB for 61.56-nm wavelength spacing. Further increasing the pump spacing results in a response nonuniformity of more than 3 dB and the 3-dB bandwidth is divided into two regions. Also, the conversion bandwidth will decrease as the pump spacing increases, which is not beneficial to the wavelength conversion function. The maximum 3-dB bandwidth of 93.3 nm can be achieved just when the response nonuniformity is 3 dB.

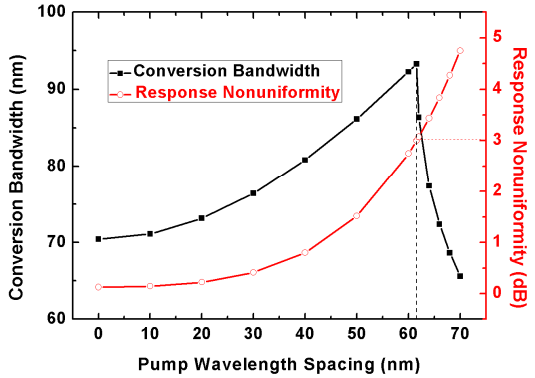

Figure 4. Conversion bandwidth and the corresponding response nonuniformity as the pump wavelength spacing varies.

The bandwidth enhancement based on two-pump FWM is experimentally demonstrated, as shown in Fig. 5 [10]. The two pumps are provided by two continuous-wave (cw) tunable lasers (Santec ECL-200) whose wavelengths are set at 1549.9 and 1564.8 nm. They are coupled through a 50/50 coupler and amplified using a high-power erbium-doped fiber amplifier (Amonics AEDFA-C-33-R), whose saturation power is around 23 dBm. The two pumps are filtered out through a demultiplexer whose central wavelength is at 1550 nm and a tunable band-pass filter, which is tuned to about 1565 nm. Another cw tunable laser (ECL-210) serves as the signal, whose output power is about 11 dBm. The pumps and signal are coupled into a 1.7-cm-long silicon waveguide with a cross section of 3 μm × 3 μm (the effective mode area is about 5 μm^2) via a 70/30 coupler. After this coupler, the powers of the two pumps and the signal are estimated to be around 13.2, 19.8, and 6.1 dBm, respectively. The coupling efficiency between the fiber and the waveguide is about

Downloaded From: http://spiedigitallibrary.org/ on 11/15/2012 Terms of Use: http://spiedl.org/terms

1.5 dB. In the silicon waveguide, FWM occurs among the two pumps and the signal, and an idler is generated. The FWM spectrum is observed using an optical spectrum analyzer (Ando AQ6317B).

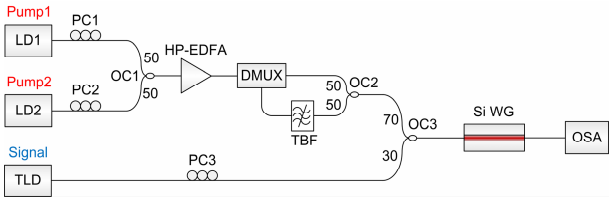

Figure 5. Experimental setup for the wavelength conversion based on two-pump FWM. TLD: tunable laser diode, PC: polarization controller, EDFA: erbium-doped fiber amplifier, TBF: tunable bandwidth filter, OC: optical coupler, and OSA: optical spectrum analyzer.

Figure 6(a) shows the measured optical spectrum of the two-pump wavelength conversion using the experimental setup in Fig. 5. Here the signal is set at 1561.4 nm and the idler is generated at 1553.2 nm, which is enlarged and shown in the inset. From Fig. 6(a), one can find that the extinction ratio of the generated idler, which is defined as the difference between peak power and the noise floor, is about 10 dB with a measured resolution of 0.01 nm. For comparison, the FWM with a single pump is also experimentally demonstrated. Here Pump1 is turned off and Pump2 is tuned to 1557.7 nm, almost equal to the central wavelength of the two pumps in the two-pump FWM. As shown in Fig. 6(b), a signal at 1561.5 nm is converted to 1553.9 nm pumped by the single Pump2.

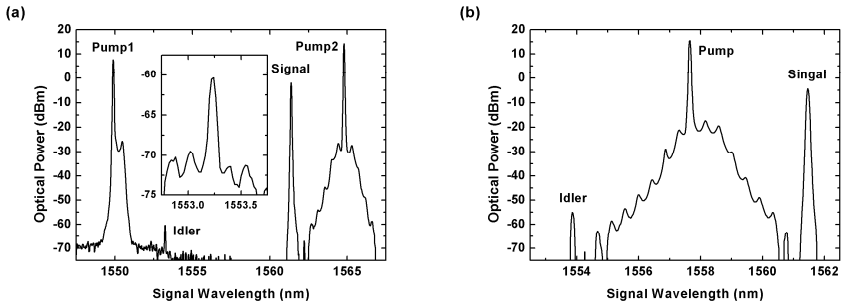

Figure 6. (a) Optical spectrum of the FWM pumped by two cw pumps at 1549.9 nm and 1564.8 nm. The inset is the enlarged description of the generated idler. (b) Optical spectrum of the FWM pumped by a single cw pump at 1557.7 nm.

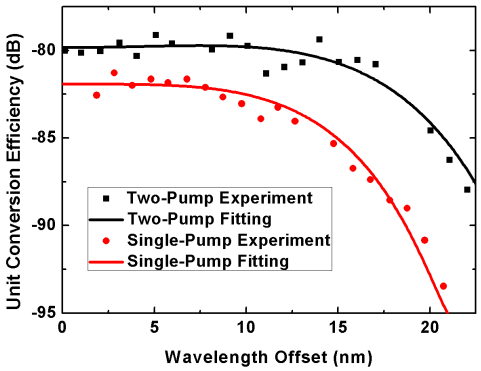

Figure 7. Measured unit conversion efficiencies and the fitting curves for the two-pump and single-pump wavelength conversions.

By scanning the signal wavelength, the response of conversion efficiency can be obtained from a series of measured FWM spectra, as shown in Fig. 7. It is known that the efficiency is tightly related to the pump powers, i.e., $\eta_{nd} \propto P_{p1}P_{p2}$ and $\eta_d \propto P_p^2$. In the experiments, the gains in the EDFA will be different for the two-pump and single-pump cases. For comparison, unit conversion efficiency is introduced by eliminating the influence of the pump powers (i.e., $\eta_{nd\text{-}unit}$ =

Downloaded From: http://spiedigitallibrary.org/ on 11/15/2012 Terms of Use: http://spiedl.org/terms

$\eta_{nd}/P_{p1}P_{p2}$ and $\eta_{d\text{-}unit} = \eta_d/P_p^2$). By fitting the measured conversion efficiencies, the experimental bandwidths are calculated from Fig. 7. The bandwidth of the single-pump FWM is 29.8 nm, while it is enhanced to 37.4 nm for the two-pump FWM. The bandwidth is improved by 25% through introducing the two-pump FWM regime.

4. TWO-PUMP FWM BASED ULTRA-BROADBAND WAVELENGTH CONVERISON

Figure 8 illustrates the ultra-broadband wavelength conversion utilizing two-pump FWM to create a dual replica of an optical signal. To achieve the phase match over a broad wavelength range, the first pump P_1 is set near the signal wave S. The second pump P_2 is set near the frequencies at which the idlers are desired. When the involved pump and signal waves are injected into a silicon waveguide, two typical two-pump FWM processes occur and two idlers are generated, which are denoted as I_1 and I_2. As shown in Fig. 8, the frequencies of the two idlers are written as $f_{I1} = f_S + f_{P2} - f_{P1}$ and $f_{I2} = f_{P1} + f_{P2} - f_S$ according to the energy conservation law, where $f_{P1,P2,S,I1,I2}$ are the frequencies of the involved waves. Correspondingly, the phase mismatches for the two FWM processes can be expressed as [11]

$$\kappa_1 = \beta_{P1} - \beta_S + \beta_{I1} - \beta_{P2} + (2\pi n_2 f_{P1}/c)I_{P1} + (2\pi n_2 f_{P2}/c)I_{P2} \tag{10}$$

$$\kappa_2 = \beta_S - \beta_{P1} + \beta_{I2} - \beta_{P2} + (2\pi n_2 f_{P1}/c)I_{P1} + (2\pi n_2 f_{P2}/c)I_{P2} \tag{11}$$

where $\beta_{P1,P2,S,I1,I2}$ are the wave numbers of the corresponding signals, n_2 is the nonlinear index coefficient, and $I_{P1,P2}$ are the pump intensities. As shown in Fig. 8, the first pump P_1 is very close to the signal S and the small frequency spacing between the first pump and the signal is denoted as Δf. Due to the law of conservation of energy in FWM processes, the idlers I_1 and I_2 will also have frequency spacing $\pm\Delta f$ between the second pump P_2. Therefore, the wave number differences between the adjacent interacting waves β_S and β_{P1} (also $\beta_{I1,I2}$ and β_{P2}) are small regardless of the actual wavelength of P_2. As long as Δf is small enough to minimize $\beta_{P1} - \beta_S$, the total phase mismatches will be low for high-efficiency wavelength conversion over an ultra-broad conversion bandwidth.

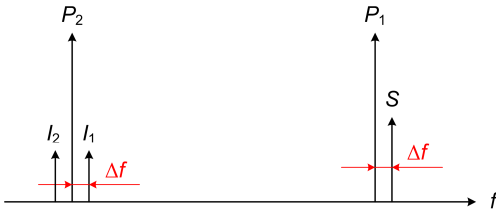

Figure 8. Principle of ultra-broadband one-to-two wavelength conversion based on nondegenerate FWM.

In above analysis, the waveguide dispersion profile is not taken into account. In fact, the influence of waveguide dispersion will be slight and the phase mismatch can be controlled to be low once the first pump is set close to the signal according to Eqs. (10) and (11). As a result, ultra-broad bandwidth can be achieved in spite of the waveguide characteristics, which is quite convenient for realizing practical ultra-broadband wavelength converters.

Proof-of-concept simulations are performed by using silicon waveguides with different geometries and hence different dispersion profiles. Particular waveguide parameters are derived for four silicon waveguides with dimensions of 300 × 500 nm^2, 300 × 650 nm^2, 285 × 650 nm^2, and 3 × 3 μm^2 by using beam propagation method. In these simulations, the linear loss of the silicon waveguides is assumed to be 0.7 cm^{-1}, the two-photon absorption coefficient is 0.8 cm/GW, the free carrier lifetime is 2 ns, and the nonlinear index coefficient is 9×10^{-18} m^2/W. Both of the incident pump intensities are assumed to be 100 mW/μm^2 and the signal intensity is 10 mW/μm^2. According to the ITU WDM channel grid, the first pump P_1 is set at 1543.73 nm (Ch42) and the signal S is at 1542.94 nm (Ch43). By scanning the wavelength of the second pump P_2, Fig. 9 shows the phase mismatch and the corresponding conversion efficiency, which is defined as the ratio of the generated idler power with respect to the incident signal power: $\eta = P_{I1,I2\text{-}out}/P_{S\text{-}in}$. The phase mismatch and efficiency for the idler I_1 are shown in Figs. 9(a) and 9(b). It is shown that the phase mismatch can be controlled to be within ±2 cm^{-1} for a wavelength region of >550 nm in 17-mm-long silicon waveguides with different dimensions. As a result, the conversion response exhibits an ultra-broad bandwidth. The 3-dB bandwidth is calculated from Fig. 9(b) to be subsequently 630 nm, 604 nm, 535 nm, and 558 nm for the above mentioned waveguides, respectively. For the idler I_2 shown in Fig. 9(c), the phase mismatch almost has an opposite sign compared with the idler I_1 as the linear phase mismatches in Eqs. (10) and (11) are approximately opposite and the intensity-induced phase mismatches are small.

Downloaded From: http://spiedigitallibrary.org/ on 11/15/2012 Terms of Use: http://spiedl.org/terms

Therefore, the conversion response of the idler I_2 in Fig. 9(d) is almost the same as that of the idler I_1 in Fig. 9(b) and an ultra-broad bandwidth can also be predicted, that is, the one-to-two ultra-broadband wavelength conversion can be achieved using this method.

As demonstrated above, the realization of the ultra-broad bandwidth depends on the small frequency spacing Δf between the signal S and the first pump P_1. If the frequency spacing is increased, the differences between β_S and β_{P1} (also $\beta_{I1,I2}$ and β_{P2}) will also increase. As a result, the phase mismatch will increase rapidly and the conversion bandwidth will decrease. By keeping the pump P_1 at 1543.73 nm (Ch42) and tuning the signal S from 1542.94 nm (Ch43) to 1540.56 nm (Ch46) in the 3 × 3 μm^2 waveguide, the influence of the frequency spacing can be observed, as shown in Fig. 10, where the idler I_1 is taken as the example. From Fig. 10(a), one can find that the phase mismatch is enlarged when the signal S goes far away from the pump P_1, and the corresponding conversion bandwidth is reduced dramatically. As shown in Fig. 10(b), the 3-dB bandwidth reduces from 558 nm to 159 nm for the signals at ITU WDM channels of Ch43-46 (558 nm, 309 nm, 210 nm, and 159 nm), respectively.

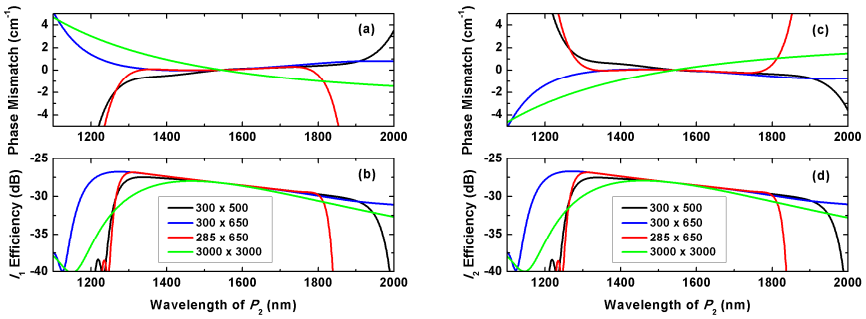

Figure 9. Calculated phase mismatch and conversion efficiency for the two generated idlers in 300 × 500 nm^2, 300 × 650 nm^2, 285 × 650 nm^2, and 3 × 3 μm^2 silicon waveguides. (a) I_1 phase mismatch; (b) I_1 conversion efficiency; (c) I_2 phase mismatch; (d) I_2 conversion efficiency.

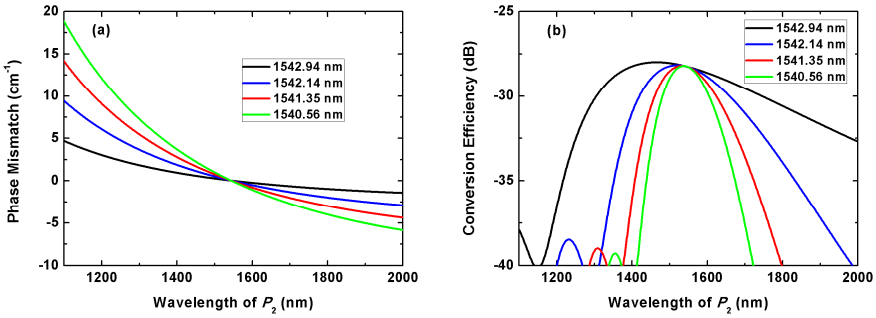

Figure 10. Simulation results of (a) the phase mismatch and (b) the conversion efficiency of the idler I_1 for different signal wavelengths as the pump P_2 scans and the pump P_1 is fixed at 1543.73 nm.

Theoretical predictions are tested at telecommunication wavelengths in the experimental setup shown in Fig. 11. The first pump P_1 and the signal S are produced by two continuous-wave tunable lasers (Santec ECL-200). They are coupled together via a 50/50 coupler and amplified by a high-power erbium-doped fiber amplifier (Amonics AEDFA-C-33-R). After eliminating the amplified spontaneous emission noise using a tunable band-pass filter (its bandwidth is about 2 nm and can let P_1 and S pass simultaneously), the first pump P_1 and the signal S are coupled into a 17-mm-long silicon waveguide with 5 μm^2 effective mode area together with the second pump P_2, which is produced by another continuous-wave tunable laser (Santec ECL-210), through a 70/30 coupler. In the silicon waveguide, the two FWM processes analyzed in section 2 occur and two idlers I_1 and I_2 are generated. They are observed using an optical spectrum analyzer (Ando AQ6317B). By scanning the second pump P_2, the signal S can be converted to the idlers in different wavelength regions.

The measured optical spectra are shown in Fig. 12, where the first pump P_1 is set at 1543.64 nm and the signal is set at 1542.83 nm [Figs. 12(a)-12(d)] or 1542.05 nm [Figs. 12(e)-12(h)], whose wavelength spacing to the pump P_1 is around 0.8 nm or 1.6 nm. For the 1542.83-nm signal, Fig. 12(a) shows the spectra of the first pump P_1 and the signal S. The

Downloaded From: http://spiedigitallibrary.org/ on 11/15/2012 Terms of Use: http://spiedl.org/terms

spectra of the second pump P_2 and the generated idlers $I_{1,2}$ are shown in Figs. 12(b)-12(d) when P_2 is tuned to 1560nm, 1595 nm, and 1630 nm, respectively. It is noticeable that the generated idler powers are almost unchanged when scanning the wavelength of the pump P_2, which indicates an ultra-broad conversion bandwidth. Unfortunately, the tunable laser we used for the pump P_2 in our experiment has a limited tuning range from 1530 nm to 1630 nm and the FWM effects can not be measured for the pump P_2 beyond 1630 nm. Figures 12(e)-12(h) show the spectra for the 1542.05-nm signal, which are quite similar to Figs. 12(a)-12(d) expect for the enlargement of wavelength spacing between the two idlers and the second pump. Moreover, the idler powers are a little smaller than those for the 1542.83-nm signal because a larger phase mismatch is introduced when the signal S moves away from the pump P_1.

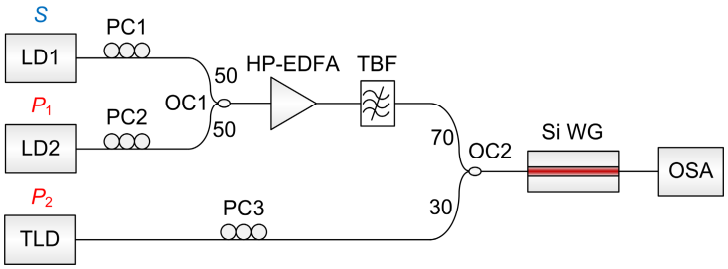

Figure 11. Experimental setup for ultra-broadband one-to-two wavelength conversion.

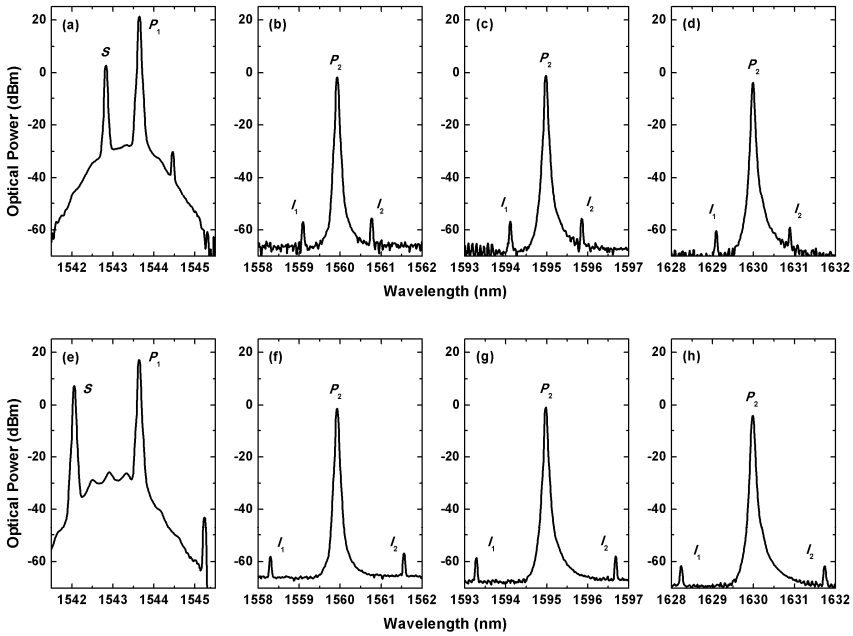

Figure 12. Measured optical spectra for the signal at 1542.83 nm or 1542.05 nm when the pump P_1 is set at 1543.64 nm. (a) The pump P_1 and the 1542.83-nm signal; (b)-(d) the pump P_2 and the generated idlers $I_{1,2}$ when the pump P_2 is at 1560 nm, 1595 nm, and 1630 nm corresponding to (a); (e) the pump P_1 and the 1542.05-nm signal; (f)-(h) the pump P_2 and the generated idlers $I_{1,2}$ when the pump P_2 is at 1560 nm, 1595 nm, and 1630 nm corresponding to (e).

In order to quantitatively evaluate the performance of the proposed wavelength conversion, the conversion efficiency is measured. For the convenience of comparison, we introduce a unit conversion efficiency to eliminate the effect of the pump powers, which is defined as $\eta_{unit} = \eta_{appro}/(P_{P1}P_{P2})$ and the approximate conversion efficiency η_{appro} is the ratio of the output idler power with respect to the output signal power: $\eta_{appro} = P_{I1,I2\text{-}out}/P_{S\text{-}out}$. With such definitions, Fig. 13 shows the unit conversion efficiency calculated from the measured output FWM spectra. As indicated in Fig. 13, the unit conversion efficiency for each idler (I_1 or I_2) varies very slight when the wavelength of pump P_2 changes. The experiment data are fitted and the efficiency difference within 100 nm (1550-1650 nm) is only 0.8 dB and 1.5 dB for the 0.8-nm and 1.6-nm wavelength spacing respectively. The entire 3-dB bandwidth can not be measured due to the tuning

Downloaded From: http://spiedigitallibrary.org/ on 11/15/2012 Terms of Use: http://spiedl.org/terms

range of the pump laser. However, the prediction from the measured efficiency data agrees well with the theoretical analysis and the ultra-broadband wavelength conversion performance can also be verified.

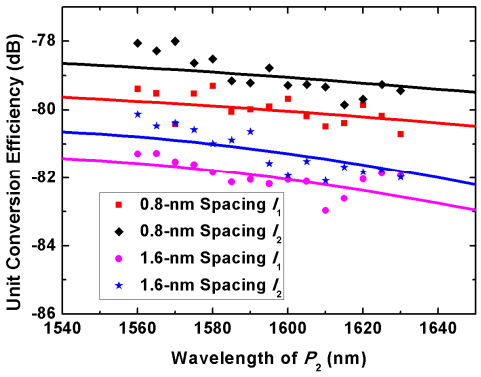

Figure 13. Measured unit conversion efficiencies of the two idlers and their fitting curves as the pump P_2 scans for the 1542.83-nm and 1542.05-nm signals that have 0.8-nm and 1.6-nm spacing with the pump P_1.

5. CONCLUSION

The nondegenerate FWM with two pumps in silicon waveguides have been theoretically and experimentally investigated for the applications in broadband wavelength conversion. It has been demonstrated that the two pump FWM has more flexible phase-matching condition and are easy to realize bandwidth enhancement in comparison to the single-pump FWM. Also, by setting one pump near the signal and scanning the other pump, once can achieve an ultra-broad conversion bandwidth of more than 500 nm and it can almost cover the entire optical communications bands. This work may provide more references to the real application of silicon-based wavelength converters in the next generation optical communication systems.

ACKNOLWDGEMENT

This work was supported by the National Natural Science Foundation of China (Grant No. 60978026), the Zhejiang Provincial Natural Science Foundation of China (Grant No. Y1090379), and the National High Technology Research and Development Program of China (863 Program) (Grant No. 2011AA010301).

REFERENCES

[1] Yoo, S. J. B, "Wavelength conversion technologies for WDM network applications," J. Lightwave Technol. 14(6), 955-966 (1996).

[2] Inoue, K. and Toba, H., "Wavelength conversion experiment using fiber four-wave mixing," IEEE Photon. Technol. Lett. 4(1), 69-72 (1992).

[3] Geraghty, D. F., Lee, R. B., Verdiell, M., Ziari, M., Mathur, A., and Vahala, K. J., "Wavelength conversion for WDM communication systems using four-wave mixing in semiconductor optical amplifiers," IEEE J. Sel. Top. Quantum Electron. 3(5), 1146-1155 (1997).

[4] Fukuda, H., Yamada, K., Shoji, T., Takahashi, M., Tsuchizawa, T., Watanabe, T., Takahashi, J., and Itabashi, S., "Four-wave mixing in silicon wire waveguides, " Opt. Express 13(12), 4629-4637 (2005).

Downloaded From: http://spiedigitallibrary.org/ on 11/15/2012 Terms of Use: http://spiedl.org/terms

[5] Lin, Q., Zhang, J., Fauchet, P. M., and Agrawal, G. P., "Ultrabroadband parametric generation and wavelength conversion in silicon waveguides," Opt. Express 14(11), 4786-4799 (2006).
[6] Liu, X., Green, W. M. J., Chen, X., Hsieh, I.-W., Dadap, J. I., Vlasov, Y. A., Osgood Jr, R. M., "Conformal dielectric overlayers for engineering dispersion and effective nonlinearity of silicon nanophotonic wires," Opt. Lett. 33(24), 2889-2891 (2008).
[7] Espinola, R. L., Dadap, J. I., Osgood, R. M., McNab, S. J., and Vlasov, Y. A., "C-band wavelength conversion in silicon photonic wire waveguides," Opt. Express 13(11), 4341-4349 (2005).
[8] Park, J. S., Zlatanovic, S., Cooper, M. L., Chavez-Boggio, J. M., Divliansky, I. B., Alic, N., Mookherjea, S., and Radic, S., "Two-pump four-wave mixing in silicon waveguides," Frontiers in Optics, OSA Tech. Dig., FML2 (2009).
[9] Gao, S., Li, Z., Tien, E.-K., He, S., and Boyraz, O., "Performance evaluation of nondegenerate wavelength conversion in a silicon nanowire waveguide," J. Lightwave Technol. 28(21), 3079-3085 (2010).
[10] Gao, S., Tien, E.-K., Huang, Y., and He, S., "Experimental demonstration of bandwidth enhancement based on two-pump wavelength conversion in a silicon waveguide," Opt. Express 18(26), 27885-27890 (2010).
[11] Gao, S., Tien, E.-K., Song, Q., Huang, Y., and Boyraz, O., "Ultra-broadband one-to-two wavelength conversion using low-phase-mismatching four-wave mixing in silicon waveguides," Opt. Express 18(11), 11898-11903 (2010).

Downloaded From: http://spiedigitallibrary.org/ on 11/15/2012 Terms of Use: http://spiedl.org/terms